Applied Mathematical Modelling 36 (2012) 1359–1370

Contents lists available at SciVerse ScienceDirect

Applied Mathematical Modelling

journal homepage: www.elsevier.com/locate/apm

Numerical modeling of surge overtopping of a levee

Jeremy A. Sharp [a,*], William H. McAnally [b]

[a] US Army Engineering Research and Development Center Coastal, Hydraulics Lab River Engineering Branch, 3909 Halls Ferry Road, Vicksburg, MS 39183, United States
[b] Department of Civil Engineering, 235 Walker Engineering Building, MS 39762, United States

ARTICLE INFO

Article history:
Received 13 January 2011
Received in revised form 8 August 2011
Accepted 16 August 2011
Available online 5 September 2011

Keywords:
Levee
Overtopping
Numerical modeling
Adaptive Hydraulics Model

ABSTRACT

Levee protection/armoring is critical in flood fighting, and understanding the flow characteristics involved requires the evaluation of the overtopping processes with a variety of tools. The Adaptive Hydraulics Model (AdH) is used to calculate velocity and depth during an overtopping event. Using these values, the work explores the application of AdH for the estimation of associated shear stresses, so that appropriate measures are applied for protection to ultimately reduce the probability of levee failure during an overtopping event. Four different depths and three Manning's *n* values were used for a total of twelve different test cases. Results show mean shear stress increases with increased surge depth and roughness. Additionally, the area of greatest shear stress is shown to be at the slope transitions from levee to berm. Values calculated in this effort should be considered in the design and implementation of levee protection.

Published by Elsevier Inc.

1. Introduction

In recent years many researchers [1–3] have implemented numerical models to simulate wave overtopping. Work conducted by Reeve et al. [4] explored the effects of combined wave and surge overtopping discharge in a numerical flume by applying the 3-dimensional Reynolds Averaged Navier–Stokes, RANS, equations with a finite difference scheme. The model used was a modified model of RIPPLE and a turbulence model that had been expanded to solve complex free surfaces [5], since the model originally was developed in 2-dimensional form by Lin and Liu [6]. In the 3-dimensional form, Reeve et al. [4] found that the "majority of the numerical model results were slightly larger than the corresponding predictions from empirical equations" [4, p. 161]. Reeve et al. [4] accounted for this discrepancy by the fact that flow acceleration might be underestimated with the use of the simple linear superposition [4]. Further validation of the numerical model was done using experimental data results from [7,8]. Although the work included the simulation of several slopes, and surge and wave overtopping events, Reeve et al. [4] expressed the need for further experiments that would include determination of the velocities experienced on the structure.

Beyond numerical model studies, most levee overtopping work has been conducted with physical models. Hughes [9], Hughes and Nadal [10], Nadal and Hughes [11] ran experiments on a physical model at USACE ERDC-CHL in Vicksburg, Mississippi. In the work conducted by Hughes and Nadal [10], a physical scale model (scaled 25:1) of a levee section with a flood-side slope of 1:4.25 and a protected side slope of 1:3 was used with 27 different combinations of wave and surge overtopping scenarios. Seven pressure cells along with two laser doppler velocimeters were used to measure the overtopping events. This setup allowed the measurements of velocities, depth, and acceleration at each pressure cell. With multiple instruments and experiments, post-processing data is the most time consuming aspect of this type of physical modeling.

* Corresponding author. Tel.: +1 601 618 9699; fax: +1 601 634 4158.
E-mail addresses: Jeremy.A.Sharp@usace.army.mil (J.A. Sharp), Mcanally@cee.msstate.edu (W.H. McAnally).

0307-904X/$ - see front matter Published by Elsevier Inc.
doi:10.1016/j.apm.2011.08.039

Nomenclature

τ_o	shear stress
γ_w	specific weight of water
h	flow thickness perpendicular to the slope
S_f	frictions lope
θ	angle of levee slope to horizontal
s	down-slope coordinate
v	flow velocity parallel to the slope
g	acceleration of gravity
t	time
η_m	mean unsteady flow depth
R	hydraulic radius
ρ	fluid density
u	flow velocity in the x-direction
v	flow velocity in the y-direction
h	flow depth
g	gravitational acceleration
z_b	bed elevation
n	Manning's roughness coefficient
σ	Reynolds stress
C_f	*friction coefficient*

Physical modeling results of the overtopping process are critical in the validation of the numerical models. Likewise, validated numerical models can fill gaps in physical model studies due to limitations of instruments, and they also provide a means of applying a large set of varying domain conditions. However, in numerical modeling the physics are limited to the equations implemented; therefore, it is important to have data that accurately represents the true behavior of the system without assumed simplifications. The issues/concerns associated with previous experiments by Reeve et al. [4] need addressing, and the flexibility of Adaptive Hydraulics (AdH) modeling allows exploration of key issues. The objective of this work is twofold:

- Validate numerical model with respect to the physical modeling of surge overtopping done by Hughes and Nadal [10].
- Explore changes in landward-side levee face shear stresses due to levee berm effects and variations in slope roughness.

Achievement of the objective is outlined in a three-phase process via the use of a numerical flume model. This paper presents work done in the first phase, and it is recommended that the following phases be conducted in future work. Future phases should use 3-dimensional AdH modeling to solve for wave and surge overtopping using both the shallow water equations and the Navier–Stokes equations. Use of the 2-D model will result in the raw output of depth and velocity magnitudes for surge overtopping at multiple locations on the landward side levee face. This overcomes issues with pressure cell and velocity meter limitations in the physical model study. Shear stresses are estimated from the results of AdH using the same equations implemented by Nadal and Hughes [11].

2. Levee grid

The grid is a 15.24 m wide and 609.6 m long flume with a slope of 0.0005 m/m. The transition zone from the berm to the flume slope, or steep to mild slope, imposes a hydraulic jump which prevents the transfer of backwater effects into the domain. A flat flume slope would perform likewise, but would not provide an efficient means of removing excess water from the transition zone. Additionally, the grid has a 152.4 m radius bulb at the end of the flume. The bulb is used to reduce reflection and upstream flow effects. At the upstream end, the boundary condition is specified as a water surface elevation. The levee section is in the first third of the flume and has a 1:4 flood-side slope and a 1:3 protected-side slope. Berms are on both sides of the levee and are sloped at 1:20. Shown in Fig. 1 are the plan and oblique views of the model's mesh.

Simulations are varied by changing the surface roughness coefficient and varying the total surge depth. In all, twelve different combinations are evaluated using a Manning's n of 0.0125, 0.02, and 0.035, and a surge depth of 0.6096, 0.9144, 1.219, and 1.524 m. In the work conducted by [11], Manning's n ranged from 0.012 to 0.04. The following is a list of the possible variation in material based on the selected Manning's n values:

- 0.0125 = Steel Surface, Cement, Wood [12].
- 0.02 = Stone in Mortar, Excavated Earth [12], Gravel [13].
- 0.035 = High Grass, Smooth Rocks [12].

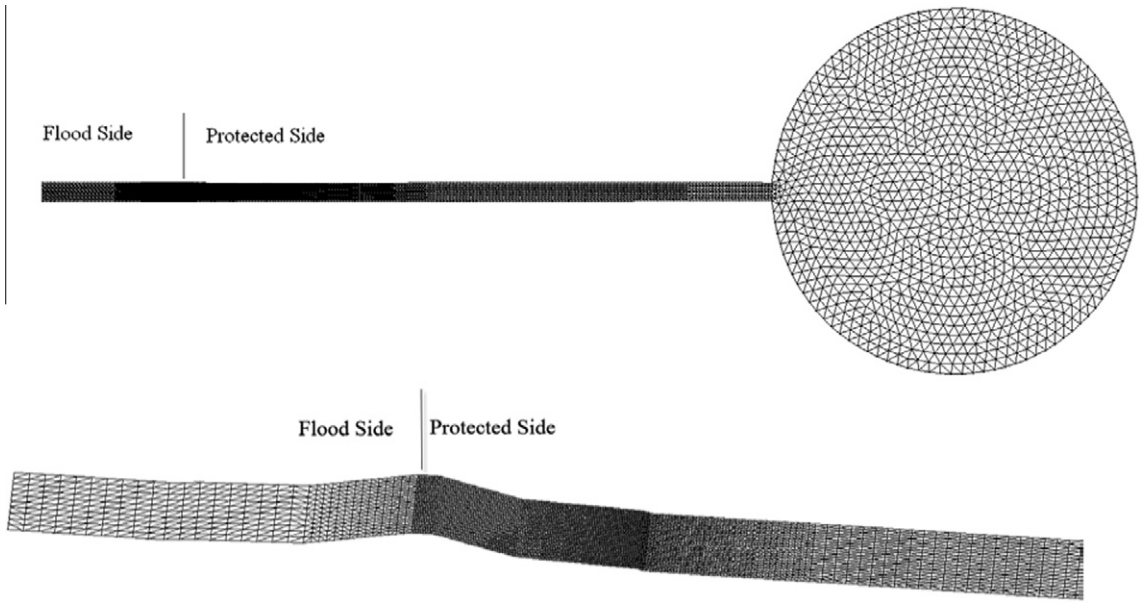

Fig. 1. Plan (top) and oblique (bottom) views of AdH mesh.

The selection of a Manning's n is based on experience [12], and the above values are only a few possible examples that might be appropriate for simulating skin friction on a levee slope. Prior to the implementation of these results it is recommended that the roughness ratio or hydraulic radius divided by roughness height, be estimated and be less than 276 or greater than 4.32. If it falls outside this range then the Manning's roughness approximation is not valid for the levee cover [12].

3. Adaptive Hydraulics Model (AdH)

As mentioned, the equations solved for in the 2-dimensional shallow water module of AdH are the 2-dimensional nonlinear shallow water equations as described in [14,15,7,16]. These equations have proven successful in describing non-breaking wave conditions [4]. The equations are derived with the assumption that the vertical velocity component is negligible. For this study, the primary application is to simulate a steady state, surge-only flow; therefore, it is assumed that the equations are applicable for the given conditions.

Neglecting shear stress and fluid pressure at the free surface, the 2-dimensional shallow water equations as implemented within AdH are written as:

$$\frac{\partial Q}{\partial t}+\frac{\partial F_x}{\partial x}+\frac{\partial F_y}{\partial y}+H=0, \tag{1}$$

where

$$Q=\begin{Bmatrix} h \\ uh \\ vh \end{Bmatrix}, \tag{2}$$

$$F_x=\begin{Bmatrix} uh \\ u^2h+\frac{1}{2}gh^2-h\frac{\sigma_{xx}}{\rho} \\ uvh-h\frac{\sigma_{yx}}{\rho} \end{Bmatrix}, \tag{3}$$

$$F_y=\begin{Bmatrix} vh \\ uvh-h\frac{\sigma_{yx}}{\rho} \\ v^2h+\frac{1}{2}gh^2-h\frac{\sigma_{yy}}{\rho} \end{Bmatrix} \tag{4}$$

and

$$\mathbf{H} = \begin{Bmatrix} 0 \\ gh\dfrac{\partial z_b}{\partial x} + n^2 g \dfrac{u\sqrt{u^2+v^2}}{h^{1/3}} \\ gh\dfrac{\partial z_b}{\partial y} + n^2 g \dfrac{v\sqrt{u^2+v^2}}{h^{1/3}} \end{Bmatrix}. \tag{5}$$

The Reynolds stresses (σ), where the first subscript indicates the direction, and the second indicates the face on which the stress acts, are due to turbulence. The Reynolds stresses are determined using the Boussinesq approach to the gradient in the mean currents:

$$\sigma_{xx} = 2\rho\nu_t \frac{\partial u}{\partial x}, \tag{6}$$

$$\sigma_{yy} = 2\rho\nu_t \frac{\partial v}{\partial y}, \tag{7}$$

and

$$\sigma_{xy} = \sigma_{yx} = 2\rho\nu_t \left(\frac{\partial u}{\partial y} + \frac{\partial v}{\partial x}\right). \tag{8}$$

Here ν_t = kinematic eddy viscosity, which varies spatially where turbulence closure is achieved through the algebraic eddy viscosity formulation described by Rodi [17].

The equations are discretized using the finite element method in which u, v, and h are represented as linear polynomials on each element.

The system of partial differential equations represented in Eq. (1) is solved with the finite element method described in [18] using the approach of Petrov–Galerkin that incorporates a combination of a Galerkin test function and a non Galerkin component to control oscillations due to convection [19].

AdH utilizes a Pseudo-Transient Continuation and Switched Evolution Relaxation inspired time step size selection algorithm [20]. This technique computes the optimal time step size dependent on the L2 norm of the system of equations.

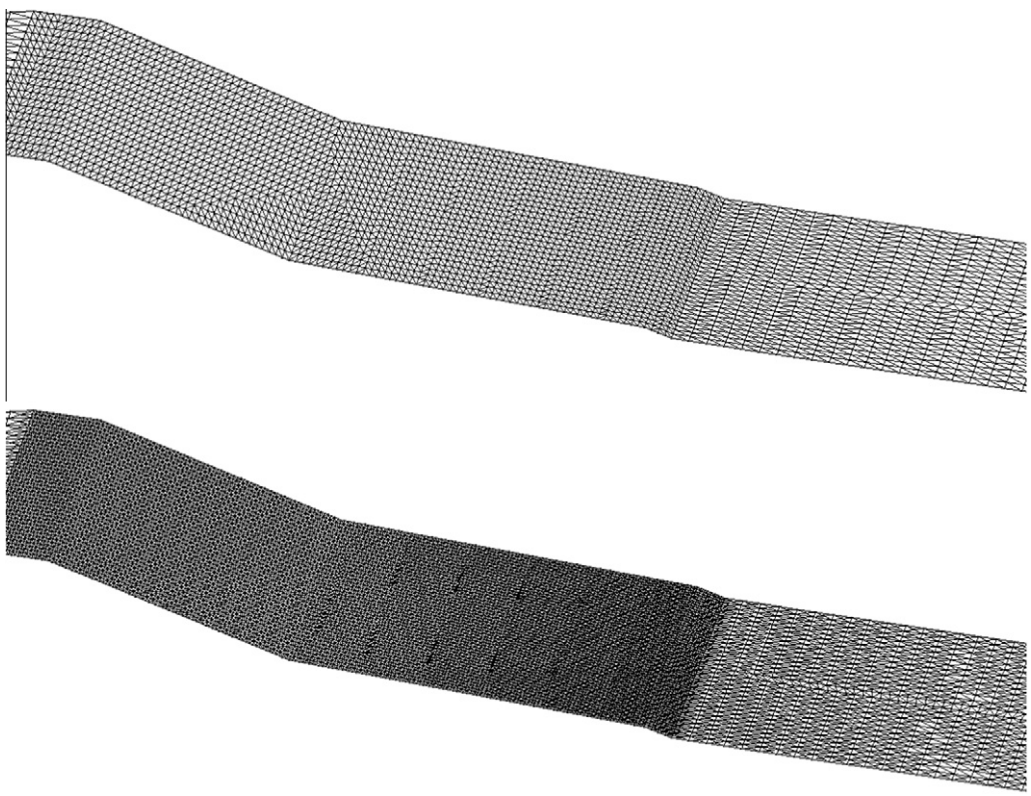

Fig. 2. Adaptive mesh comparison of protected side of levee, adaption 0 (top) and adaption 2 (bottom).

This selection algorithm provides an efficient technique for temporally accurate solution of rapidly varying hydrodynamic and sediment flows. Additional information about the AdH model can be accessed in the cited references and at https://adh.usace.army.mil/.

In most numerical model studies a grid convergence test is typically conducted prior to model validation. AdH enables the user to forgo the cumbersome task of grid convergence with the use of an adaptive mesh. "As its name implies, AdH applies mesh adaption techniques, which are based on the normal of the continuity equation residual integrated over the element and computed for each time step, to refine and coarsen a mesh based on flow complexity" [21, p. 5]. "If the residual is larger than the refinement tolerance, the element will be refined (split in half); otherwise, no adaption occurs." [21, p. 8]. Adaption eliminates the need for the construction of multiple grids with varying resolution that are then compared to determine the most appropriate mesh based on both resolution and run time. AdH adaption details can be found in [14].

Although not necessary for most applications, the authors used 5 different levels of adaption to ensure the model was properly simulating the hydromechanics of the surge event. Adaption 0, the base mesh, consists of 6300 nodes. The number denoted in the name of each mesh indicates the number of times the mesh can adapt in the area of interest, the area of the protected side slope, i.e., adaption 0 adapts zero times. From adaption 0; adaption 1, adaption 2, adaption 3, and adaption 4, were used with a 0.6096 m surge event to determine the best convergent and time efficient mesh. Outside the area of interest, the unprotected side and downstream in the flume, the model was allowed to adapt one time for adaption 1–3. However, in order to determine the impacts of the surrounding mesh on the area of interest, in adaption 4 the surrounding mesh was set to an adaption of two. Adaption 1, adaption 2, adaption 3, and adaption 4 adapt approximately to 12,000, 18,000, 21,000 and 23,000 nodes respectively (see Fig. 2).

It is shown that this increased resolution does decrease the amount of residual error (see previous paragraph for error definition) used for setting the refinement parameters (see Fig. 3). However, adaption 4 doubled the runtime and, when compared to the other levels of adaption, the velocity and depth profile did not produce a significant enough difference to justify the less computationally efficient model.

With complex flow conditions in levee overtopping events validation ensures that the model represents the true behavior of the process. Model validation is achieved using results from empirical equations and physical model measurements reported by [22,10,8]. For the most part discharges calculated with AdH were shown to be at or near that of the weir equation for the 0.6096 and 0.9144 m surge events. The 1.219 and 1.524 m surge event discharges are greater than the weir equation. Conversely, the [9,22] results showed a greater discharge than that of AdH for the 0.6096 and 0.9144 m surges and the 1.219 and 1.524 m surge events agreed more closely to the AdH results (see Fig. 4).

The velocity comparison between the numerical and physical model showed close agreement. Unfortunately, at the lower surge depth of 0.61 m the velocity meters were suspect of measuring erroneous and inconsistent velocity data and could not be used for comparison [15]. The available velocity data, shown at PG 4 and PG 7, was captured at two different surge depths

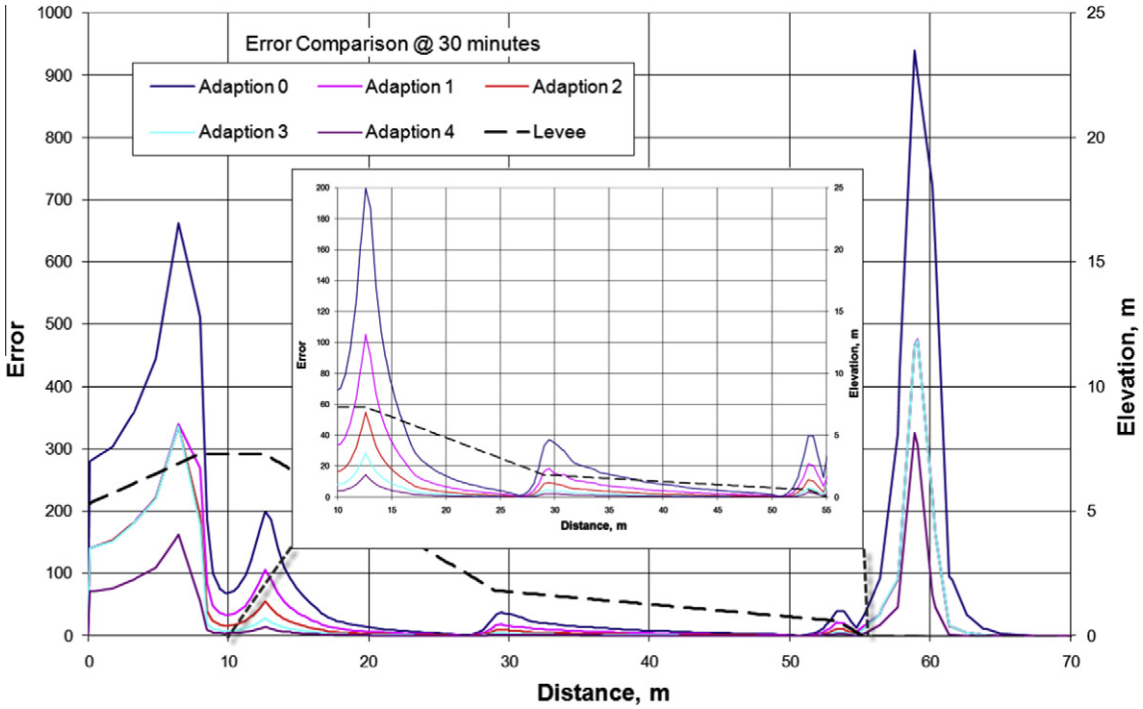

Fig. 3. Comparison of residual error for different levels of adaption.

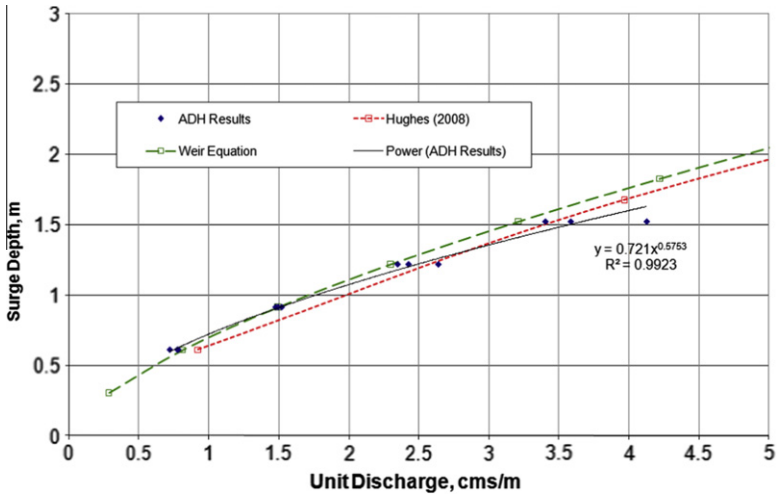

Fig. 4. Comparison of unit discharge.

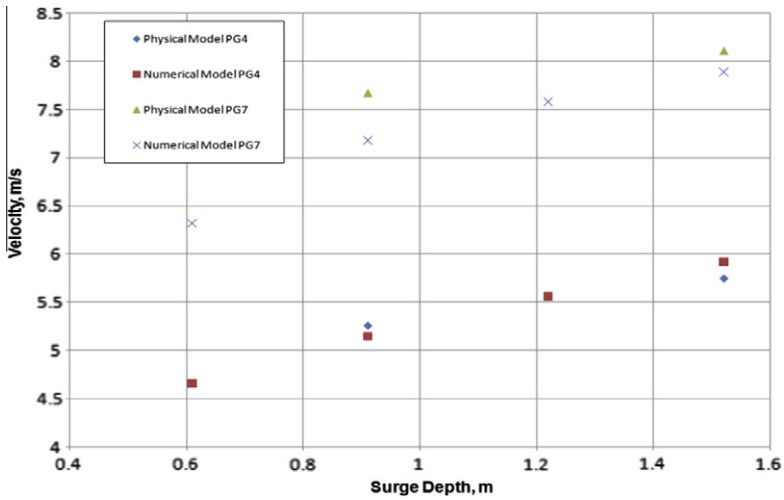

Fig. 5. Comparison of velocity at locations of physical model gages.

0.91 and 1.52 m. For the case of the 0.91 m surge both gages in the physical model measured a velocity that is higher than that of the numerical model (see Fig. 5). Variation between the two models at PG 4 and PG 7 is 2% and 6%, respectively. Similarly, at a 1.52 m surge depth variation at PG 4 and PG 7 is −2% and 2% respectively. This indicates a closer agreement for the two models at the higher surge depth. It is the judgment of the authors that an agreement within 10% or less is sufficient for validation for the purposes of this application.

4. Calculations

For estimating shear stress experienced on the protected side levee face due to the non-uniform and unsteady overtopping flow the 1-D momentum equations applicable to steep slopes was implemented. From [11]:

$$S_f = \frac{\tau_o}{\gamma_w h} = \sin\theta - \frac{\partial h}{\partial s} - \frac{\partial}{\partial s}\left(\frac{v^2}{2g}\right) - \frac{1}{g}\frac{\partial v}{\partial t}. \tag{9}$$

The unknown variables are depth and velocity. This work took a three step approach to the shear stress analysis. First, an approximation assuming steady-state flow reduces the momentum equation to the weight of the water offset by the bottom shear stress as shown in Eq. (10):

$$\tau_{o,\text{mean}} = \gamma_w \eta_m \sin\theta. \tag{10}$$

Next, the momentum equation, with the acceleration term between two points was implemented to produce Eq. (11). Note that Nadal and Hughes [11] mistakenly omitted the velocity term that is part of the convective acceleration in Eq. (11). Therefore, the Nadal and Hughes [11] shear stress estimates based on the incorrect version of Eq. (11) are invalid [11]:

$$\tau_0 = \gamma_w h\left[\sin\theta - \frac{\partial h}{\partial s} - \frac{\partial}{\partial s}\left(\frac{v^2}{2g}\right)\right]. \tag{11}$$

Including the acceleration terms in the equation results in the following form [11]:

$$\tau_0 = \gamma_w h_{12}\left[\sin\theta - \frac{\partial h}{\partial s} - \frac{\partial}{\partial s}\left(\frac{v^2}{2g}\right) - \frac{1}{g}\frac{\partial v}{\partial t}\right]. \tag{12}$$

As the final approach the full 1-D version of the momentum equation is used as shown in Eq. (12), the temporal acceleration is removed. Removal of the acceleration term is justified since the model is at steady state. As noted, "estimating the time series of shear stress using the momentum equation is difficult for these experiments because no direct measurements of flow velocity were acquired on the landward-side slope" [10, p. 248]. The numerical model overcomes this issue since AdH can solve for velocity.

Eq. (12) is invalid in areas that include zero slope, such as on the crest, and locations of rapid spatial variation, i.e., the hydraulic jumps, and slope transitions. At locations of rapid spatial variations, Eq. (12) will often exhibit a negative shear stress indicating a flow reversal, which obviously is not the case in a 2-dimension depth-averaged model. Eq. (13) [23] is implemented where Eq. (12) is invalid:

$$\tau = 1/2\rho C_f v^2, \tag{13}$$

$$C_f = \frac{2gn^2}{(1.49R^{1/6})^2}. \tag{14}$$

Using Eq. (12), estimated average shear stresses on the protected face of the levee are shown in Fig. 6; which, show less agreement to [9] estimated results than the estimates of unit discharges. Note: Hughes [9] estimated that the Manning's n for the prototype surge cases of 0.3048, 0.9144, and 1.524 m were 0.0115, 0.0262, and 0.0381 respectively. Since the shear stresses are estimated based on calculations from AdH, velocity results are dependent on surface friction, error is amplified. However, the shear stresses show similarity to experimental [9] results as shown in Fig. 6. Here it is shown that the physical model results fall between those of the numerical model and are most similar to the AdH results using a Manning's n of 0.035. This is possibly the result of both an over-prediction in the discharge at lower flows and under-prediction of discharge at higher flows as shown in the difference between unit discharge of the physical model and numerical model (see Fig. 4).

Rather than presenting a mean shear stress for the protected side slope, this study presents a shear stress profile such that critical failure points on the levee are identified. Areas of transition present the greatest degree of equation limitation and a case by case base evaluation (application of the equations is dependent on the geometry so a different levee section might require a slight variation in the application of shear equations) is required to implement the correct equation for the specific location. The equations implemented are Eqs. (12) and (13). Eq. (12) is applied for gradually varying flow, and is applicable for the majority of the protected side of the levee cross-section. Eq. (13) is ideal for steady uniform flow and can be used if the velocity and depth are changing (see Fig. 7). Where Eq. (12) fails Eq. (13) is used.

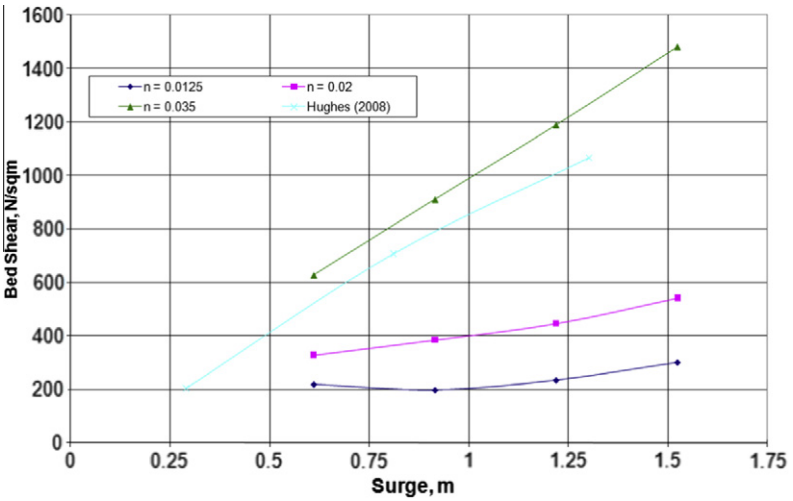

Fig. 6. AdH bed shear compared to [9] results.

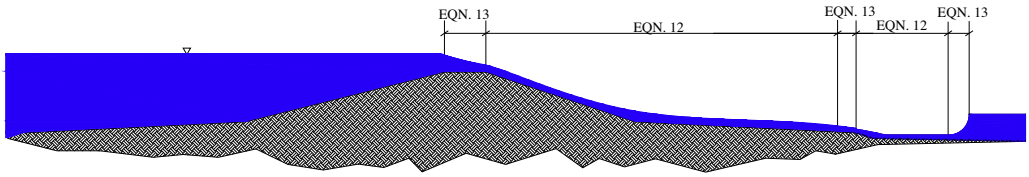

Fig. 7. Location of applied shear stress equations.

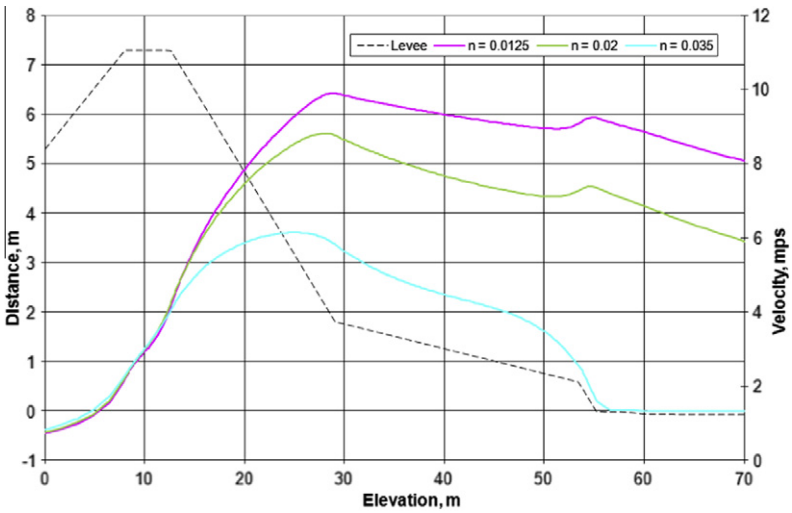

Fig. 8. Velocity profiles for a 1.22 m surge with varying Manning's *n*.

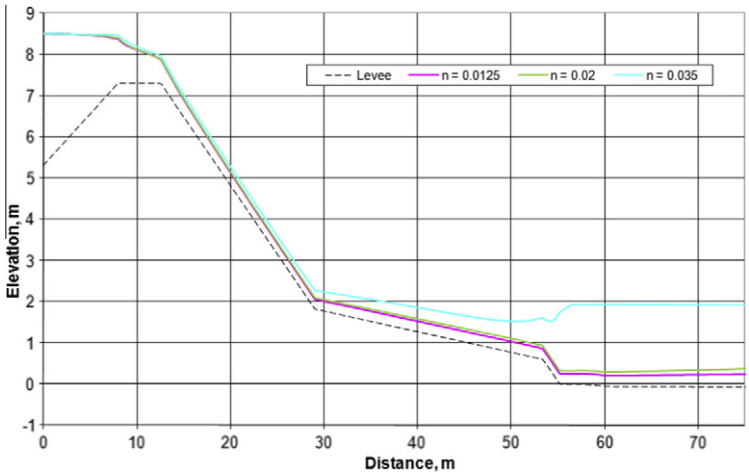

Fig. 9. Water surface profiles for a 1.22 m surge with varying Manning's *n*.

5. Results

Physical and numerical model results show that velocity profiles vary with respect to location on the levee cross-section. A single point velocity or mean velocity is misleading in an overtopping analysis, because of the rapid spatial variations in velocity. Since the evaluation is analyzing a steady state flow condition, the model is allowed to reach steady state converging in approximately 3 min, and the velocity profiles 15 min into the simulation are used. This time was selected to avoid both initial unsteady and later downstream backwater conditions that could affect the velocity profile. From the levee crest to the protected side levee toe, the velocity profile increased. Velocity profiles indicated a velocity maximum at or near the landward side levee slope toe. A secondary local maximum of lower magnitude occurred at or near the toe of the berm, so velocity inflection points occur at abrupt changes in slope. These maximums are unlikely since a real world levee would have

smoother transitions. As expected for uniform flow, a greater roughness results in greater flow depth and lower velocity, as expected from the energy equation and illustrated in Figs. 9 and 8. Furthermore, although results are not shown here, as surge depth on the unprotected side increased so did the corresponding velocities. All functions of the velocities should be carefully considered when evaluating a protective measure.

The water surface profile (Fig. 9) is more intuitive since it follows basic hydraulic logic. At the crest the water surface behaves as a broad crested weir. Moving down the levee slope the depth gradually decreases as the potential energy is transformed to kinetic energy and attempts to reach a terminal velocity. At the levee and berm slope transition, the flow deepens and continues to deepen until it runs off the berm where a hydraulic jump forms directly after or slightly downstream. At a Manning's n of 0.035 the jump will form above the end of the berm with a Manning's n of 0.02 the jump occurs slightly inland of the berm. With a Manning's n of 0.0125 the jump is much further inland. Therefore, the higher the surge the deeper the flow depth; likewise, the rougher the levee section the deeper the flow depth.

As shown in Fig. 10 shear stress evaluation requires appropriate equation selection. In the Figure each equation yields vastly different results and appropriate application is imperative for the correct calculation of bed shear in its corresponding location. Some, such as the one on the crest, are wildly incorrect; therefore, ultimately in this work, the bed shear is estimated using a combination of Eqs. (12) and (13), both shown in Fig. 10, at different locations on the levee as shown in Fig. 7.

Fig. 11 illustrates the resulting bed shear stress profile as calculated with Eqs. (12) and (13) combined spatial as illustrated in Fig. 6, and is the best estimate for the shear stress profile. The lower Manning's n is used as an illustration since

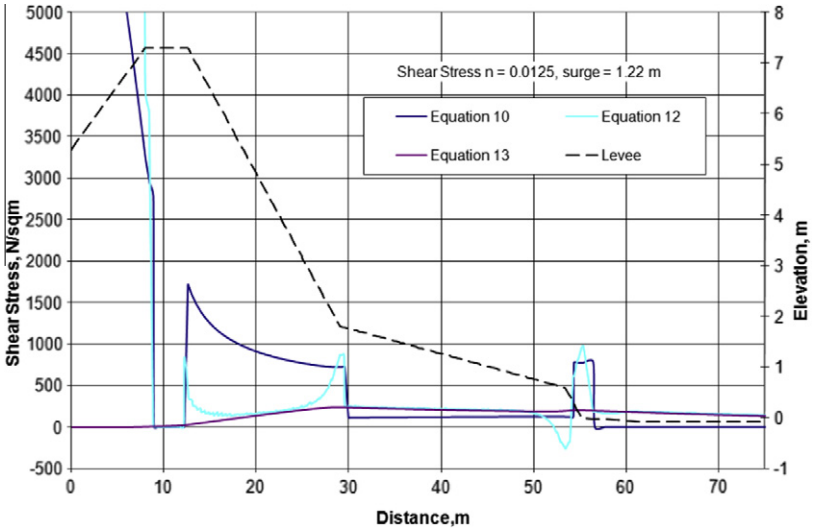

Fig. 10. Shear stress of all four equations with respect to location on the levee.

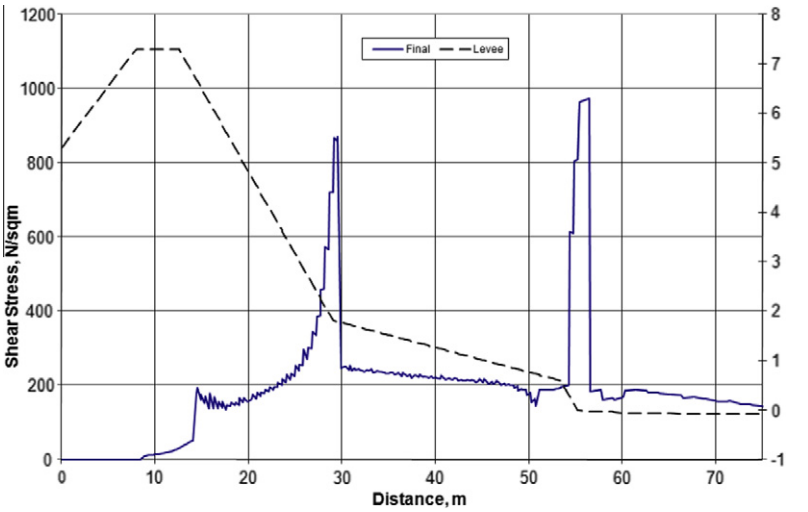

Fig. 11. Combined shear stresses of Eqs. (12) and (13) for surge of 1.22 and n = 0.0125.

Table 1
Mean bed shear for the levee protected side slope.

Surge (m)	Bed shear (N/m^2)		
	$n = 0.0125$	$n = 0.02$	$n = 0.035$
0.61	218.19	327.74	627.17
0.91	197.48	384.62	910.63
1.22	233.66	446.01	1188.72
1.52	300.20	541.46	1480.98

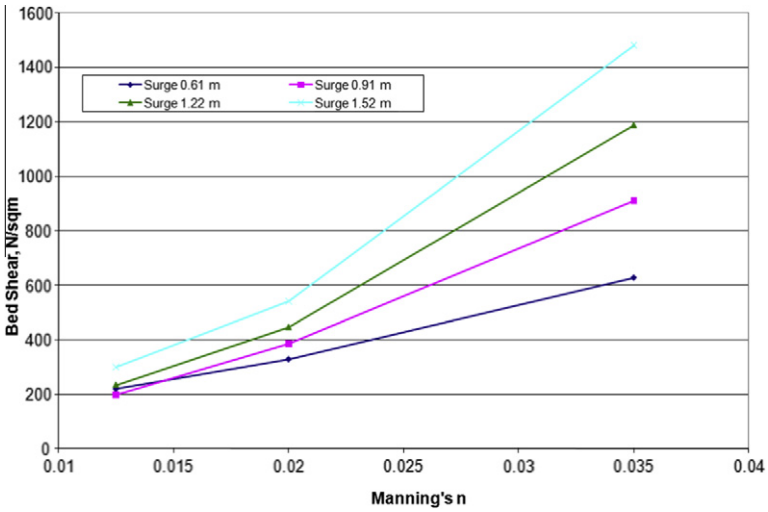

Fig. 12. Mean bed shear for the levee protected side slope.

it closely represents the surface friction of a geo-fabric that is being tested to determine the feasibility of it for armoring a levee prior to overtopping.

The following table shows the mean shear stress behavior with respect to surge depth and Manning's *n*. The mean shear stress represents an average for the entire protected side levee slope.

As shown in Table 1 and Fig. 12, shear stress increases with both surge and increasing Manning's number. For a comprehensive understanding of the erosive nature during the initial stages of levee failure peak shear stress values are essential. Shown in the best estimated shear stress profile Fig. 11, it is evident that the greatest areas of shear stress are at the transitions from the levee-berm and then from the berm to flume bed. The highest magnitude at the levee and berm transition occurred in the most extreme case of a 1.52 m overtopping event Fig. 13. However, at the berm to flume transition, with

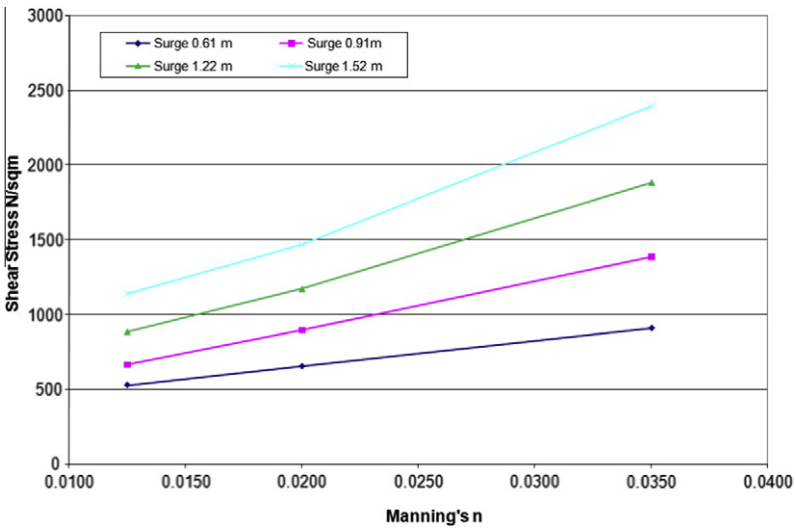

Fig. 13. Peak shear at levee berm transition 21.04 m from crest.

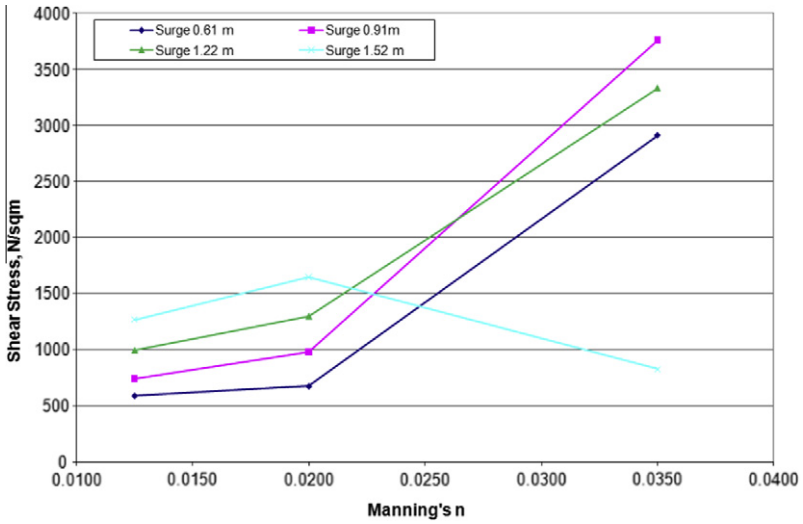

Fig. 14. Peak shear at berm flume transition 46.92 m from crest.

increasing depth the flow overcame the skin drag decreasing the shear peak for the higher surge events, as shown in the reversed downward trend of the highest surge in Fig. 14.

6. Conclusion

The work was validated with average shear stress, velocity, and discharge comparisons to [9,22,15] physical models. Validation provides a level of confidence in that the results are reasonable, illuminating a few key points. First, the 2-dimensional form of AdH appears adequate to produce reasonable results. The 2-dimensional AdH model provides an option for other levee geometries; however, it is recommended to only evaluate shallower slopes, those less than 1:3, on the protected side of the levee. Additionally, a numerical model is more easily applied for different geometries than that of a physical model. Secondly, lower surge events were shown at the berm to flume transition on the levee to produce greater shear stresses than that of higher surge events when the surface friction coefficient (Manning) was equal to 0.035. That effect is caused by a hydraulic jump forming at the base of the berm, which was permitted in the numerical experiments but not in the physical experiments. For events that are less than 0.91 m, it appears that protective measures, if only based on shear, can be designed based on the lower surge event being considered, since concurrent increases in surges which are less than 0.91 m, results in proportionate increase in shear. However, for events greater than 0.91 m both the "higher" event and a range of lower events should be considered for the proper design and assessment of defensive measures for protected-side levee slopes, in particular at slope transitions.

Velocity and shear stresses seem to be greatest at locations of transitions. The transitions were modeled conservatively in this paper, in that they were abrupt changes in slope resulting in the maximum local shear stress. Understanding the maximums ensures that forces on the levee during overtopping events are not underestimated. Therefore, abrupt changes are the most ideal in investigating protective measures to counteract shear forces exerted on a levee during an overtopping event. If levee protection measures are designed to the maximum occurring shear stresses across the entire protected side then levee failure probability is reduced.

Role of the funding source

The authors would like to acknowledge the support and funding from SERRI who supported this effort. The paper is in direct support of the Mississippi State University lead project "Increasing Community Disaster Resilience through Targeted Strengthening of Critical Infrastructure (Rapid Repair)". Sponsors had no other role in the submission or execution of this paper.

Disclosure statement

Currently there are no known potential conflicts of interest for either author. It would like to be known that the first author did the associated work while working for Mississippi State University in the Civil and Environmental Engineering Department.

Acknowledgements

This research was funded by the Department of Homeland Security and sponsored by the Southeast Region Research Initiative (SERRI) at the Department of Energy's Oak Ridge National Laboratory. This research was performed under Project Number 70015 through Mississippi State University and principal investigator Isaac L. Howard.

Special thanks are extended to Dr. Gaurav Savant, Dynamic Solutions, LLC, and Dr. Charlie Berger, US Army Corp of Engineers Engineering Research and Development Center, Coastal and Hydraulics Lab (USACE ERDC-CHL). Without their expertise in AdH and modifications to the code this simulation would not be possible. Additional thanks to Dr. Steven Hughes, USACE ERDC, CHL, for providing guidance and for his work associated with this project.

References

[1] D. Causon, D. Ingram, C. Mingham, J. Zang, K. Hu, J.G. Zhou, Numerical simulation seawall overtopping, in: Proceedings of the 27th International Conference on Coastal Engineering, Sydney, Australia, 2000, pp. 2086–2099.
[2] k. Hu, C.G. Mingham, D.M. Causon, Numerical simulation of wave overtopping of coastal structure using the non-linear shallow water equation, Coast. Eng. 41 (2000) 433–465.
[3] M.E. Hubbard, N. Dodd, A 2D numerical model of wave run-up and overtopping, Coast. Eng. 47 (2002) 1–26.
[4] D.E. Reeve, A. Soliman, P.Z. Lin, Numerical study of combined overflow and wave overtopping over a smooth impermeable seawall, Coast. Eng. 55 (2008) 155–166.
[5] P. Lin, W. Xu, NEWFLUME: a numerical water flume for the tow dimensional turbulent free surface flows, J. Hydraul. Res. 44 (1) (2006) 79–93.
[6] P. Lin, P.L.-F. Liu, A numerical study of breaking waves in the surf zone, J. Fluid Mech. 359 (1998) 239–264.
[7] A. Soliman, Numerical Study of Irregular Wave Overtopping and Overflow, Ph.D. Thesis, The University of Nottingham, United Kingdom, 2003.
[8] A. Soliman, D.E. Reeve, Numerical study for small negative freeboard wave overtopping and overflow of sloping sea wall, in: Proceedings of 3rd International Conference of Coastal Structures, 2003, Portland, Oregon, American Society of Civil Engineering, New York, 2004, pp. 643–655.
[9] S.A. Hughes, Combined Wave and Surge Overtopping of Levees: Flow Hydrodynamics and Articulated Concrete Mat Stability, US Army Engineering Research and Development Center, 2008. TR-08-7.
[10] S.A. Hughes, N.C. Nadal, Laboratory study of combined wave overtopping and storm surge overflow of a levee, Coast. Eng. 56 (2009) 244–259.
[11] N.C. Nadal, S.A. Hughes, Shear Stress Estimates for Combined Wave and Surge Overtopping at Earthen Levees, US Army Engineering Research and Development Center, 2009. CHETN-III-79.
[12] T.W. Sturm, Open Channel Hydraulics, McGraw-Hill Higher Education, New York, 2001.
[13] P.Y. Julien, River Mechanics, Cambridge University Press, Cambridge, UK, 2002.
[14] R.C. Berger, J.N. Tate, G.L. Brown, G. Savant, Adaptive Hydraulics User Manual, A Two-Dimensional Modeling System Developed by the Coastal and Hydraulics Laboratory, US Army Engineering Research and Development Center, 2010.
[15] J.M. Shaw, Shear Stress Analysis of Levees Subjected to Combined Surge and Wave Overtopping, Master Thesis, Mississippi State University, 2010.
[16] J.N. Tate, R.C. Berger, R.L. Stockstill, Refinement indicator for mesh adaption in shallow-water modeling, Journal of Hydraulics Engineering – ASCE (2006) 854–857.
[17] W. Rodi, Turbulence Models and their Application in Hydraulics – A State of the Art Review, Balkema, Leiden, 1993.
[18] G. Savant, R.C. Berger, T.O. McAlpin, J.N. Tate, Efficient implicit finite-element model for dam and levee breach, Journal of Hydraulic Engineering – ASCE (2011), doi:10.1061/(ASCE)HY.1943-7900.0000372.
[19] R.C. Berger, HIVEL 2D v2.0 Users Manual, Waterways Experiment Station, US Army Corps of Engineers, MS 39180, 1997.
[20] G. Savant, C. Berger, T. McAlpin, J. Tate, Application of Adaptive Hydraulics (ADH) to Rapidly Evolving Hydrodynamic Flows, System Wide Water Resource Program, TN-SWWRP-10.6, US Army Engineering Research and Development Center, 2010.
[21] E.A. Hammack, D.S. Smith, R.L. Stockstill, Modeling Vessel-Generated Currents and Bed Shear Stress, US Army Engineering Research and Development Center, Vicksburg, MS, 2008. TR-08-7.
[22] S.A. Hughes, J.M. Shaw, Continuity of instantaneous wave overtopping discharge with application to stream power concepts, Journal of Waterway, Port, Coastal, and Ocean Engineering 137 (1) (2011) 12–25.
[23] W.H. McAnally, E. Hayter, Boundary Stresses and Velocity Profiles in Estuarine Flows, Technical Report, DRP-92-3, Waterways Experiment Station, Vicksburg, MS, 1992.